[Title Page]

Pyrolysis of Chinese chestnut shells: Effects of temperature and Fe presence on product composition

Sunwen Xia[a], Kaixu Li[a], Haoyu Xiao[a], Ning Cai[a], Zhiguo Dong[a], Chen xu[a],

Yingquan Chen[a,*], Haiping Yang[a,*], Xin Tu[b], Hanping Chen[a]

a State Key Laboratory of Coal Combustion, Huazhong University of Science

and Technology, Wuhan, Hubei, 430074, China

b Department of Electrical Engineering and Electronics, University of Liverpool,

L69 3GJ Liverpool, UK

E-mail: xiawen@hust.edu.cn, li_kaixu@hust.edu.cn, x_hy@hust.edu.cn,

caining@hust.edu.cn, dzghust@hust.edu.cn, chxu@hust.edu.cn,

chenyingquan@hust.edu.cn, yhping2002@163.com, xin.tu@liv.ac.uk

hp.chen@163.com

Correspondence information: Haiping Yang; 1037 Luau Road, Wuhan, Hubei

430074, P. R. China; yhping2002@163.com;

Tel., 086+027-87542417-8211; Fax, 086+027-87545526

1

Pyrolysis of Chinese chestnut shells: Effects of temperature and Fe presence on product composition

Sunwen Xia[a], Kaixu Li[a], Haoyu Xiao[a], Ning Cai[a], Zhiguo Dong[a], Chen xu[a], Yingquan Chen[a], Haiping Yang[a,*], Xin Tu[b], and Hanping Chen[a]

[a]*State Key Laboratory of Coal Combustion, Huazhong University of Science and Technology, Wuhan, Hubei 430074, China*

[b]*Department of Electrical Engineering and Electronics, University of Liverpool, L69 3GJ, Liverpool, UK*

Abstract

To understand the role of Fe on biomass pyrolysis, Fe-catalyzed biomass pyrolysis in a fixed-bed reactor was investigated. It was found that the introduction of Fe increased the yields of gases and solid char while decreasing the yield of liquid oil. With increasing temperature, Hydrogen content in gaseous products obtained in the presence of Fe increased, while that of CH_4 decreased. In the case of liquid oil, the introduction of Fe promoted the formation of ketones and acids at 400–600 °C, and these species became dominant (67.51 %) at 700–800 °C. Finally, solid char obtained in the presence of Fe at 700–800 °C featured a larger pore volume, specific surface area, and graphitization degree, and was characterized by a mesoporous structure with narrow pores size distribution (~5.3 nm).

Keywords: biomass, pyrolysis, iron, mesoporous carbon, pyrolytic polygeneration

1. Introduction

The increasing consumption of fossil fuels results in severe environmental pollution and energy shortages, necessitating the search for alternative fuels. In this regard, biomass appears to be the most promising substitute of fossil resources for applications such as heat/power production and transportation (Kan et al., 2016; Tripathi et al., 2016; Wang et al., 2017b) and can additionally be converted into different chemicals and biomaterials (Li et al., 2015). For example, pyrolysis of biomass, which has already been performed on an industrial scale, can be used to produce liquid fuels, chemicals, and biomaterials (Chen et al., 2019b). However, the further development of biomass pyrolysis is hindered by the fact that this technique affords products with suboptimal properties, e.g., pyrolytic gas with low H_2 content and high CO content (Ail et al., 2016), oil with high oxygen content (Chen et al., 2017a), and amorphous biochar with low porosity (Liu et al., 2015).

Consequently, various additives and catalysts have been investigated to enhance the quality of biomass pyrolysis products. Chen et al. (Chen et al., 2017a) studied the pyrolysis of cotton stalk, showing that the addition of CaO increased the yields of CH_4 and H_2 while decreasing that of CO_2. Mochizuki et al. (Mochizuki et al., 2013) found that when Jatropha residue pyrolysis was performed in the presence of SiO_2, the formation of oxygenated compounds (e.g., acids, ketones, and aldehydes), coke, and polycyclic aromatic compounds was inhibited. In addition, ZSM-5, a widely studied catalyst for bio-oil deoxygenation, was shown to significantly decrease the oxygen content (from ~39% to 20.7–27.3%) of liquid deoxygenation products by promoting the

3

conversion of oxygen-containing organic compounds to aromatics (Chen et al., 2019a; Hernando et al., 2018). Wang et al.(Wang et al., 2017a) probed the effects of KCl on the pyrolysis of carboxymethyl cellulose, demonstrating that biochar obtained in the presence of this salt had a hierarchical pore structure, a specific surface area of 1773 m^2/g, and a specific pore volume of 1.31 m^2/g. However, the above additives and catalysts enhanced the properties of only one product type (gas, oil, or biochar), whereas the properties of all three product types need to be enhanced to make the operation of biomass pyrolytic poly-generation systems economically reasonable.

Iron has recently attracted increased attention as a biomass pyrolysis additive. For example, Dong et al. found that the addition of Fe(III) promotes the formation of non-condensable gases (mainly at the expense of liquid products) (Dong et al., 2017), while Lu et al. found that the use of Fe additives can reduce the content of oxygenated compounds and increase that of hydrocarbons such as PAHs (Lu et al., 2010). Collard et al.(Collard et al., 2012) investigated influence of impregnation with Fe on the pyrolysis of biomass constituents at 600 °C, demonstrating that this treatment decreased the yield of oxygenated compounds and increased that of H_2. Furthermore, Fe was found to promote the graphitization degree of solid char (Glatzel et al., 2013; Ōya et al., 1982). Overall, the above results indicate that as a biomass pyrolysis additive, Fe can affect the compositions and yields of tri-state products and plays an important yet not fully clear role in biomass pyrolysis. In addition, temperature is an important parameter in biomass pyrolysis and catalyst pyrolysis process. It affects products distribution and performance of catalyst (Hu et al., 2015). However, the combined effects of Fe and temperature on

4

the properties of pyrolysis products and the influence of Fe on the biomass pyrolysis

mechanism have not been fully clarified. To bridge this gap and produce high hydrogen

content gaseous, highly valued oil, and highly graphitization mesoporous char, we

herein study the pyrolysis of Chinese chestnut shells in the presence and absence of Fe

in a fixed-bed reactor at different temperatures and investigate the mechanism of Fe on

the product formation and biomass pyrolysis process. The obtained results shed light on

the role of Fe at variant temperatures and are expected to provide valuable guidance for

biomass utilization.

2. Materials and methods

2.1 Materials

Chinese chestnut shells (collected in Xiaogan, Hubei province, China) were

crushed and sieved to obtain a powder with a particle size of <2 mm. Proximate analysis

of the samples was carried out in a TGA-2000 analyzer (Las Navas, Spain), and

ultimate analysis was carried out with a CHN/O elementary analyzer (vario MICRO

cube, Elementar, Germany). This powder contained 44.68 wt% C, 5.54 wt% H, 44.69

wt% O, and 0.59 wt% N on a dry basis, and proximate analysis of a dry sample

indicated that it contained 71.73 wt% volatiles, 4.50 wt% ash, and 23.77 wt% fixed

carbon (Xia et al., 2018). To eliminate ash, the powder was impregnated with excess

hydrochloric acid for 24 h, filtered, washed with deionized water until neutrality, and

dried at 105 °C for 24 h. The ash content of the thus treated samples was determined as

0.2 wt%, which was sufficiently low to allow the effects of ash to be neglected.

Fe-containing biomass was obtained by impregnating demineralized biomass (1 g) in aqueous iron (Ⅲ) nitrate (40 mL, 0.025 M) followed by overnight drying at 150 °C in air. As a result, Fe ions were well dispersed in and adsorbed on biomass because of its fibrous structure and hydrophilic functional groups.

2.2 Pyrolysis

Schematic diagram of biomass pyrolysis system was shown at Fgure 1. Biomass was pyrolyzed in a fixed-bed reactor system that was described in our previous work and comprised a feeding unit, a vertical tube (600 mm height, 45 mm inner diameter), an electric furnace, a condensing system, and a gas cleaning and drying unit. Prior to each trial, a biomass sample (~2 g excluding the weight of ferric oxide) was placed in a quartz basket located at the top of the reactor, and the system was purged with N_2 for 30 min. The reactor was pre-heated, and once the temperature was stabilized at the selected value, the quartz basket was quickly lowered to the center of the reactor and held for 30 min. The samples were heated about 8 °Cs, and the released volatiles were carried in a flow of N_2 (200 mL/min). Condensable volatiles were liquefied in an ice-water condenser, and non-condensable ones were purified by passing through water, dried over silica gel, and finally collected in a gas sampling bag. To obtain solid char, the reactor was rapidly cooled to ambient temperature in a flow of N_2 after each trial using a cooling fan.

The solid char yield was determined as the ratio of washed char and biomass (excluding iron) weights. The liquid oil yield was determined from the weight gain of

the condensation system after pyrolysis. The yield of gaseous products was calculated

by considering their combined volume, as outlined in our previous work (Chen et al.,

2012). The volume of carried gas was determined by a mass flow controller, and gas

mean density was measured using micro-gas chromatography (micro-GC)-based gas

component analysis. All experiments were repeated three times, and the relative error of

these measurements did not exceed 5%.

2.3 Characterization of pyrolysis products

Gaseous products were analyzed using a dual-channel micro gas chromatograph

(Micro-GC 3000A, Agilent Technologies, USA) equipped with thermal conductivity

detectors. Column A (5-Å molecular sieve, Ar carrier gas) was used to analyze H_2, CO,

and CH_4 at 95 °C, while column B (ProapakQ-PPQ, He carrier gas) was used to analyze

CO_2, C_2H_6, C_2H_4, and C_2H_2 at 60 °C. Each sample was tested at least three times, and

the results were reported as averages.

The main organic constituents of liquid oil were identified by gas

chromatography-mass spectroscopy (GC-MS, HP7890 gas chromatograph equipped

with an HP5975 MS detector) using an Agilent HP-5MD capillary column (19091s-433;

30 m × 0.25 mm i.d. × 0.25 μm d.f.). The injector temperature and carrier gas (He) flow

rate equaled 300 °C and 1 mL/min, respectively, and the split ratio was set to 20:1. A

sample injection volume of 1 μL was employed. The GC oven was held at 40 °C for 3

min, then heated to 150 °C at 5 °C/min, further heated to 300 °C at 10 °C/min, and

finally held at 300 °C for 10 min. Mass spectrometry scanning was performed in the *m/z*

range of 30–500, and organic compounds were identified using the mass spectral library of the National Institute of Standards and Technology (NIST2011).

Ultimate analysis of solid char was carried out using a CHNS/O elemental analyzer (vario MICRO cube, Elementar, Germany). The surface porosity of solid char was analyzed by physisorption of N_2 at 77 K using a Quantachrome autosorb-IQ instrument (China). Specific surface areas (S_{BET}) were calculated according to the Brunauer-Emmett-Teller method. Pore size distributions were determined by applying a nonlocal density functional theory (NLDFT) method to nitrogen adsorption data and using a slit pore/cylindrical pore hybrid model. The total pore volume was determined at a relative pressure (P/P_0) of 0.99. Micropore surface areas were determined from the corresponding t-plots (Wu et al., 2017). Sample morphology was examined by scanning electron microscopy (Nova NanoSEM 450, FEI, the Netherlands) at an acceleration voltage of 10 kV.

The crystal structure and phase composition of solid char were determined by X-ray diffraction (XRD; X'Pert PRO, PANalytical B.V., the Netherlands) analysis that was performed at a scanning step of 0.026° in the 2θ range of 5–80°. Peaks were identified using the High Score Plus software package (Yao et al., 2017).

3. Results and discussion

3.1 Effects of Fe and temperature on product distribution

Figure 2 shows the distribution of pyrolysis products obtained at various temperatures. In the absence of Fe, the main products were solid char (39 wt%) and

8

liquid oil (38 wt%), while the yield of gaseous products was very low (<15 wt% at 400 °C), which was indicative of fast biomass decomposition. As the temperature increased from 400 to 800 °C, the char yield decreased from 38.8 to 25.4 wt%, while the yield of liquid oil increased to a maximum value of 52.3 wt% at 500 °C and then decreased. Furthermore, the yield of gaseous products slowly increased from 14.5 to 16.2 wt% as the temperature increased from 400 to 500 °C, with a sharp increase to 34.9 wt% observed at higher temperatures (>600 °C). This behavior was attributed to the primary decomposition of biomass and the secondary cracking of volatiles at high temperature (>500 °C) (Yang et al., 2017).

Although the presence of Fe had almost no effect on the yield of solid char (38.45 wt%) obtained at 400 °C, it decreased the yield of liquid oil (28.5 wt%) and increased that of gas (23.3 wt%), which was ascribed to the enhanced formation of small molecules in the secondary reactions of organic compounds (Filiciotto et al., 2017; Mullen et al., 2015). As the temperature increased, the distribution of products obtained in the presence of Fe evolved similarly to that obtained under Fe-free conditions. However, the yield of liquid oil was lower, while those of char and gaseous products were much higher than values obtained in the absence of Fe, e.g., the maximum yields of liquid oil and gas obtained in the presence of Fe equaled 34.6 wt% (at 500 °C) and 43.0 wt% (at 800 °C), respectively. The above results suggested that Fe, as a catalyst, promoted the cracking of volatiles to small molecules at low temperature (400 °C) and promoted aromatization reactions affording large molecules (solid char) and light gases (H_2, CO, etc.) at high temperatures (500–800 °C).

9

3.2 Properties of gaseous products

Figure 3a shows the relative yields and compositions of gases produced by biomass pyrolysis. In the absence of Fe, CO_2 was the main component (~73.3 vol%) of gaseous products at 400 °C, while its yield significantly decreased at higher temperatures, as CO_2 was mainly produced by the decarboxylation of hemicellulose at low temperatures (Wang et al., 2017b). In contrast, the yields of CH_4, CO, and H_2 increased with increasing temperature, especially in the case of CO (up to 42.1 vol%), which became the major component at 700–800 °C. This finding was attributed to the promotional effect of high temperature on dehydrogenation and the cracking of methoxy, ether, and carbonyl moieties (Chen et al., 2018).

In the presence of Fe, CO_2 was formed as the main gaseous product at low temperature (400–700 °C), with the maximal yield of 73.7 vol% observed at 400 °C. In contrast, the presence of Fe significantly affected the formation of H_2, CH_4, and CO. For example, whereas no H_2 was produced in the absence of Fe, appreciable amounts of this gas were formed in the presence of Fe even at 400–500 °C (e.g., 17.9 vol% at 500 °C), with maximal H_2 yield obtained at 800 °C. This behavior was attributed to the promotional effect of Fe on dehydrogenation reactions (Yao et al., 2018). The yields of CO and CH_4 obtained in the presence of Fe were lower than those obtained under Fe-free conditions. In addition, the LHV (Lower Heating Value) of gaseous products formed in the presence of Fe greatly increased with increasing temperature, reaching ~12 MJ/Nm^3 at 800 °C. Although this number was lower than that obtained in the

10

absence of Fe (~16 MJ/Nm^3), it was still within the range of medium heating values and exceeded the minimum threshold value of 7 MJ/Nm^3 stipulated by the Chinese National Standard for fuel gas for urban residents (Gao et al., 2017). The gas product contained higher hydrogen content and lower carbon monoxide. It can be used as fuel gas for urban residents (GB 50028-2006), also it can be used to FT synthesis for some C contained chemicals and fuels after CO_2 removing and pollutant cleaning.

Figure 3b shows the amounts of gas released during pyrolysis under various conditions. In the absence of Fe, the amount of CO_2 was almost unaffected by temperature, while the amounts of CO and CH_4 sharply increased (from 1.0 to 5.7 mmol/g and from 0.1 to 1.7 mmol/g, respectively) as the temperature increased from 400 to 800 °C. Notably, H_2 was not detected at low temperature (400–500 °C), appearing only upon a further temperature increase. In the presence of Fe, the amounts of H_2, CO, and CH_4 increased with increasing temperature, while the amount of CO_2 (~4.8 mmol/g) was not affected by temperature but significantly exceeded the value obtained in the absence of Fe (~2.5 mmol/g). This behavior could be ascribed to (i) the promotional effect of Fe on the release of CO_2 and other small molecules from organic compounds and/or (ii) the carbothermal reduction of iron oxide nanoparticles by amorphous carbon to produce CO_2. Considering that carbothermal reduction requires high temperatures (>700 °C) (Cho et al., 2016; Shen, 2015) and that the increase of CO_2 amount at low temperature was significant, we concluded that the main CO_2 formation pathway corresponded to (i). The slight decrease of CH_4 amount observed in the presence of Fe was attributed to the occurrence of Fe-catalyzed C–H bond cracking

11

(Gong et al., 2009). Finally, in the presence of Fe, H_2 was formed even at low temperature (400–500 °C), and the maximum H_2 amount (5.9 mmol/g) was 2.3 times higher than that obtained in the absence of Fe. That Fe introduction promoted the hydrogen yield is consistent with previous reference (Yao et al., 2018). As Fe might promote the deoxygenation and dehydrogenation of organic compounds and thus facilitate the release of H_2 and CO_2. The increased yield of char observed in the presence of Fe was ascribed to the condensation of dehydrogenation- and deoxygenation-produced organic compounds to form secondary char (Lu et al., 2010).

3.3 Properties of liquid oil

Liquid oil contained numerous organic constituents, and its composition was therefore difficult to quantify. However, we managed to analyze the contents of pyrolytically produced liquid oil based on the relative areas of the chromatographic peaks of 15 main components (acids, furans, ketones, phenols, sugar, and others (Table 1)). In the absence of Fe, sugars (mainly 1,6-anhydro-alpha-d-galactofuranose aka levoglucose), which were produced by the decomposition of cellulose and hemicellulose and featured high thermal stability, were the main constituents (48.24 %) of oil at 400 °C, with maximal sugar content (56.95 %) obtained at 600 °C. At higher temperatures (700–800 °C), the yield of sugars sharply decreased, whereas those of acids, furans, phenols, and ketones increased. This behavior suggested that these light oxygenates might be products of sugar decomposition, e.g., the bicyclic structure of LG could be opened through the breakage of the C–O bond between C_1 and C_2 (Xin et al.,

2013). The significant yield of acids observed at 400 °C stayed approximately constant at 400–600 °C and then sharply increased at 700–800 °C, while the yields of other oxygenated compounds (furans, phenols, ketones) decreased at 400–700 °C and then increased at 700–800 °C. Specifically, phenolics produced at low temperature (400–600 °C) mainly corresponded to 2,6-dimethoxyphenol, *p*-cresol, and 2-methoxyphenol, whereas phenol and 2-methoxyphenol were the main products formed at higher temperature (>600 °C). This finding suggested that these conditions promoted the deoxygenation reaction, which involved the removal of methoxy side chains through their reaction with radicals produced in the course of sugar cracking (Liu et al., 2015; Omoriyekomwan et al., 2016). Besides, at low temperature (400–600 °C), pyranones were the main ketones, while 1-hydroxy-2-propanone was produced (possibly via ring-opening reactions) as the main ketone at temperatures above 600 °C.

In comparison with biomass pyrolysis without Fe, the results indicated that Fe had a strong effect on the formation and speciation of sugars, acids, and other oxygenated species. For example, the introduction of Fe facilitated the production of acids and ketones but significantly decreased the yield of sugars, which first increased (maximum = 43.05 % at 500 °C) and then decreased with increasing temperature. This behavior was ascribed to the occurrence of Fe-catalyzed ring-opening, decarbonylation, and dehydrogenation reactions of sugars, which resulted in the increased production of light oxygenated compounds (ketones, acids) and low-molecular-weight gases (e.g., CO_2 and H_2; Fig. 3) (Kan et al., 2016; Wang et al., 2017b; Zakzeski et al., 2010). However, the introduction of Fe did not affect the yield of furans at low temperatures

and decreased it at high temperatures (800 °C).

In the case of phenolics, 2-methoxyphenol and phenol were mainly formed in the presence of Fe, while 2,6-dimethoxyphenol, p-cresol, and 2-methoxyphenol were produced in the absence of Fe, which suggested Fe catalyzed the removal of methoxy side chains and promoted radical reactions (Liu et al., 2015; Mouda et al., 2018; Mullen et al., 2015). Fe also promoted the formation of ketones, with the main ketone corresponding to cyclopentanone (~5.1 %). At high temperatures (>700 °C), Fe inhibited the formation of phenols, ketones, and furans while promoting the formation of acids. The generation of light oxygenated compounds were competitive relationship from cracking of LG or polymerization of fragments or radicals (Xin et al., 2013), which suggested that the introduced Fe catalyzed the formation of acids rather than that of other oxygenated compounds. This acids and ketones enriched oil has potential to synthesize biodiesel through esterification reaction. In summary, at 400-700 °C, Fe-catalyzed ring-opening, decarbonylation, and dehydrogenation reactions of sugars. It resulted in the increased production of light oxygenated compounds (ketones, acids) and low-molecular-weight gases (e.g., CO_2 and H_2; Fig. 3). In higher temperature (800 °C), Fe further promoted acids content further.

3.4 Properties of solid char

The morphology of the solid char obtained from the samples pyrolysis was examined by scanning electron microscopy (SEM). The surface of solid char obtained in the absence of Fe at 800°C was relatively smooth and flat and exhibit a gully-like

14

structure, which attributed to precipitation of volatile and the collapse of original structure. For pyrolysis with Fe, the solid char particles showed a fluffy and porous structure, with open and interconnected macro-cavities (~500nm). In higher magnification, the surface showed many worm-like structure, which consisted of sinuous, intertwined tubes with the diameters of 50nm. These sinuous tubes was named 'carbon nano-capsule', which might be produced by deposition of macromolecules on the solid surface.

Figure 4 presents a van Krevelen diagram of solid char obtained by biomass pyrolysis. The H/C and O/C ratios of solid char obtained in the absence of Fe at 400 °C equaled 0.435 and 0.122, respectively, and indicated the presence of highly condensed aromatic rings. The H/C ratio decreased with increasing temperature, while the O/C ratio initially decreased and then remained stable at 700–800 °C. This behavior agreed with the occurrence of biomass dehydrogenation and demethylation and with the increased contents of CH_4 and H_2 in gaseous products formed at 500–800 °C. In the presence of Fe, the H/C and O/C ratios of solid char evolved in a similar way but were smaller than values obtained in the absence of Fe. Therefore, the introduction of Fe was concluded to accelerate the assembly of graphitic structures, especially at high temperatures (>700 °C) (Chen et al., 2017b; Thompson et al., 2015).

The specific surface areas and pore volumes of solid products obtained at various temperatures are listed in Table 2. To describe the detailed evolution of the internal pore characteristics during pyrolysis, pore-size distributions were obtained using the NLDFT method (Figs. 5a–d). Solid char prepared in the absence of Fe

15

featured a low specific surface area (31.62 m^2/g at 400 °C) and mainly contained meso- and macropores, while no micropores were observed. With increasing temperature, a small amount of micropores was formed, which was ascribed to volatile precipitation. However, upon a further temperature increase, the surface area greatly decreased, possibly because of the collapse of the micropore structure.

When pyrolysis was performed in the presence of Fe, the specific surface area and pore volume of solid char evolved in a similar way, increasing with temperature below 600 °C. At higher temperatures, the above parameters continued to increase, with maximal S_{BET} and pore volume values (329.106 m^2/g and 0.4591 cc/g, respectively) obtained at 800 °C. At low temperatures (400–600 °C), the increase of pore volume and specific surface area was mainly caused by the development of a micropore structure, and the micropore surface area reached a maximum value of 163.928 m^2/g at 600 °C. This behavior was ascribed to the redox reactions between Fe species and the etched carbon matrix, and the formation of H_2O and CO_2 contributed to porosity development by promoting the gasification of carbon (Shen, 2015; Wang et al., 2012). At high temperature (600 °C), the increase of pore volume and specific surface area mainly reflected the development of mesopore structure. In particular, mesopore formation could be caused by (i) the overlap of micropores at high temperature and (ii) the formation of Fe carbide and elemental Fe by carbothermal reduction and the etching of the carbon matrix by the former species (Glatzel et al., 2013; Kim et al., 2017). As the external surface area reached a value of 221.754 m^2/g at 700–800 °C, and the corresponding pore size distribution was centered at 5.3 nm (mesoporous structure),

carbon matrix etching with Fe carbide was concluded to be the main mesopore formation pathway.

The degree of char graphitization was probed by XRD. For char formed in the absence of Fe at all temperatures, only one very broad peak was observed, which was indicative of an amorphous structure. However, two very broad peaks were observed for char formed in the presence of Fe at 400–600 °C, whereas the patterns of char obtained in the presence of Fe at 700–800 °C featured two obvious peaks at $2\theta = 26°$ and 43°, which were assigned to the (002) and (100) reflection of graphite. Thus, Fe was concluded to catalyze the graphitization of solid char at high temperature (700–800 °C), and the mechanism of this graphitization was suggested to involve the dissolution-precipitation of carbon atoms on the metal surface or the formation and decomposition of metal carbides (Hoekstra et al., 2016; Kim et al., 2017; Zhu et al., 2016). This highly graphitization mesoporous char can be used in the field of energy storage and water treatment (Wang et al., 2018; Zhu et al., 2018). Porosity provides a high electrode/electrolyte contact area and fast path length for ion transport. The level of graphitization is critical to promoting of electrical conductivity and durability (Sun et al., 2013). Compared graphited mesoporous carbon obtained by self-assemble method in other research (Wang et al., 2018), this highly graphitization mesoporous char from biomass have similar S_{BET} (389 m^2/g to 442 m^2/g) and pore volume (0.4591 cm^3/g to 0.75 cm^3/g).

Conclusion

Pyrolysis of Chinese chestnut shells in the presence of Fe proved to be an effective method of their utilization, and Fe was shown to play multiple roles depending on pyrolysis temperature. Specifically, Fe promoted the formation of H_2 and CO_2 and reduced the contents of oxygen-containing compounds in liquid oil formed at 400–800 °C but increasing the contents of acids. At high temperatures (700–800 °C), Fe promoted the graphitization of char and facilitated the formation of a mesoporous structure with narrow pores and a large pore volume.

Supplementary material: Supplementary data for this work can be found in the e-version of this paper.

Reference

[1] Ail, S.S., Dasappa, S., 2016. Biomass to liquid transportation fuel via fischer tropsch synthesis - technology review and current scenario. Renew. Sust. Energ. Rev. 58, 267-286.

[2] Chen, W., Chen, Y., Yang, H., Li, K., Chen, X., Chen, H., 2018. Investigation on

biomass nitrogen-enriched pyrolysis: Influence of temperature. Bioresour. Technol. 249(Supplement C), 247-253.

[3] Chen, X., Chen, Y., Yang, H., Chen, W., Wang, X., Chen, H., 2017a. Fast pyrolysis of cotton stalk biomass using calcium oxide. Bioresour. Technol. 233, 15-20.

[4] Chen, X., Chen, Y.Q., Yang, H.P., Wang, X.H., Che, Q.F., Chen, W., Chen, H.P., 2019a. Catalytic fast pyrolysis of biomass: Selective deoxygenation to balance the quality and yield of bio-oil. Bioresour. Technol. 273, 153-158.

[5] Chen, Y., Yang, H., Wang, X., Zhang, S., Chen, H., 2012. Biomass-based pyrolytic polygeneration system on cotton stalk pyrolysis: Influence of temperature. Bioresour. Technol. 107, 411-418.

[6] Chen, Y., Zhang, X., Chen, W., Yang, H., Chen, H., 2017b. The structure evolution of biochar from biomass pyrolysis and its correlation with gas pollutant adsorption performance. Bioresour. Technol.

[7] Chen, Y.Q., Liu, B., Yang, H.P., Wang, X.H., Zhang, X., Chen, H.P., 2019b. Generalized two-dimensional correlation infrared spectroscopy to reveal the mechanisms of lignocellulosic biomass pyrolysis. Proc. Combust. Inst. 37(3), 3013-3021.

[8] Cho, D.W., Lee, J., Yoon, K., Ok, Y.S., Kwon, E.E., Song, H., 2016. Pyrolysis of fecl3-pretreated spent coffee grounds using co2 as a reaction medium. Energy Conversion and Management 127, 437-442.

[9] Collard, F.X., Blin, J., Bensakhria, A., Valette, J., 2012. Influence of impregnated metal on the pyrolysis conversion of biomass constituents. Journal of Analytical and Applied Pyrolysis 95, 213-226.

[10] Dong, Q., Li, X.Q., Wang, Z.Y., Bi, Y.H., Yang, R.L., Zhang, J.F., Luo, H.Z., Niu, M.M., Qi, B., Lu, C., 2017. Effect of iron(iii) ion on moso bamboo pyrolysis under microwave irradiation. Bioresour. Technol. 243, 755-759.

[11] Filiciotto, L., Balu, A.M., Romero, A.A., Rodriguez-Castellon, E., van der Waal, J.C., Luque, R., 2017. Benign-by-design preparation of humin-based iron oxide catalytic nanocomposites. Green Chemistry 19(18), 4423-4434.

[12] Gao, Y., Wang, X., Chen, Y., Li, P., Liu, H., Chen, H., 2017. Pyrolysis of rapeseed stalk: Influence of temperature on product characteristics and economic costs. Energy 122, 482-491.

[13] Glatzel, S., Schnepp, Z., Giordano, C., 2013. From paper to structured carbon electrodes by inkjet printing. Angew. Chem.-Int. Edit. 52(8), 2355-2358.

[14] Gong, F.Y., Ye, T.Q., Yuan, L.X., Kan, T., Torimoto, Y., Yamamoto, M., Li, Q.X., 2009. Direct reduction of iron oxides based on steam reforming of bio-oil: A highly efficient approach for production of dri from bio-oil and iron ores. Green Chemistry 11(12), 2001-2012.

[15] Hernando, H., Hernandez-Gimenez, A.M., Ochoa-Hernandez, C., Bruijnincx, P.C.A., Houben, K., Baldus, M., Pizarro, P., Coronado, J.M., Fermoso, J., Cejka, J., Weckhuysen, B.M., Serrano, D.P., 2018. Engineering the acidity and accessibility of the zeolite zsm-5 for efficient bio-oil upgrading in catalytic pyrolysis of lignocellulose. Green Chemistry 20(15), 3499-3511.

[16] Hoekstra, J., Beale, A.M., Soulimani, F., Versluijs-Helder, M., van de Kleut, D.,

Koelewijn, J.M., Geus, J.W., Jenneskens, L.W., 2016. The effect of iron catalyzed graphitization on the textural properties of carbonized cellulose: Magnetically separable graphitic carbon bodies for catalysis and remediation. Carbon 107, 248-260.

[17] Hu, S., Jiang, L., Wang, Y., Su, S., Sun, L., Xu, B., He, L., Xiang, J., 2015. Effects of inherent alkali and alkaline earth metallic species on biomass pyrolysis at different temperatures. Bioresour. Technol. 192, 23-30.

[18] Kan, T., Strezov, V., Evans, T.J., 2016. Lignocellulosic biomass pyrolysis: A review of product properties and effects of pyrolysis parameters. Renew. Sust. Energ. Rev. 57, 1126-1140.

[19] Kim, D.W., Kil, H.S., Kim, J., Mochida, I., Nakabayashi, K., Rhee, C.K., Miyawaki, J., Yoon, S.H., 2017. Highly graphitized carbon from non-graphitizable raw material and its formation mechanism based on domain theory. Carbon 121, 301-308.

[20] Li, C.Z., Zhao, X.C., Wang, A.Q., Huber, G.W., Zhang, T., 2015. Catalytic transformation of lignin for the production of chemicals and fuels. Chemical Reviews 115(21), 11559-11624.

[21] Liu, W.J., Jiang, H., Yu, H.Q., 2015. Development of biochar-based functional materials: Toward a sustainable platform carbon material. Chemical Reviews 115(22), 12251.

[22] Lu, Q., Zhang, Z.-F., Dong, C.-Q., Zhu, X.-F., 2010. Catalytic upgrading of biomass fast pyrolysis vapors with nano metal oxides: An analytical py-gc/ms study. Energies 3(11), 1805-1820.

[23] Mochizuki, T., Atong, D., Chen, S.Y., Toba, M., Yoshimura, Y., 2013. Effect of sio2 pore size on catalytic fast pyrolysis of jatropha residues by using pyrolyzer-gc/ms. Catalysis Communications 36, 1-4.

[24] Mouda, P.H., Kantarelis, E., Andersson, K.J., Engvall, K., 2018. Biomass pyrolysis gas conditioning over an iron-based catalyst for mild deoxygenation and hydrogen production. Fuel 211, 149-158.

[25] Mullen, C.A., Boateng, A.A., 2015. Production of aromatic hydrocarbons via catalytic pyrolysis of biomass over fe-modified hzsm-5 zeolites. ACS Sustain. Chem. Eng. 3(7), 1623-1631.

[26] Omoriyekomwan, J.E., Tahmasebi, A., Yu, J.L., 2016. Production of phenol-rich bio-oil during catalytic fixed-bed and microwave pyrolysis of palm kernel shell. Bioresour. Technol. 207, 188-196.

[27] Ōya, A., Marsh, H., 1982. Phenomena of catalytic graphitization. Journal of Materials Science 17(2), 309-322.

[28] Shen, Y.F., 2015. Carbothermal synthesis of metal-functionalized nanostructures for energy and environmental applications. J. Mater. Chem. A 3(25), 13114-13188.

[29] Sun, L., Tian, C.G., Li, M.T., Meng, X.Y., Wang, L., Wang, R.H., Yin, J., Fu, H.G., 2013. From coconut shell to porous graphene-like nanosheets for high-power supercapacitors. J. Mater. Chem. A 1(21), 6462-6470.

[30] Thompson, E., Danks, A.E., Bourgeois, L., Schnepp, Z., 2015. Iron-catalyzed

graphitization of biomass. Green Chemistry 17(1), 551-556.

[31] Tripathi, M., Sahu, J.N., Ganesan, P., 2016. Effect of process parameters on production of biochar from biomass waste through pyrolysis: A review. Renewable and Sustainable Energy Reviews 55, 467-481.

[32] Wang, C., Wu, D., Wang, H., Gao, Z., Xu, F., Jiang, K., 2017a. Nitrogen-doped two-dimensional porous carbon sheets derived from clover biomass for high performance supercapacitors. J. Power Sources 363(Supplement C), 375-383.

[33] Wang, J., Xu, Y.L., Ding, B., Chang, Z., Zhang, X.G., Yamauchi, Y., Wu, K.C.W., 2018. Confined self-assembly in two-dimensional interlayer space: Monolayered mesoporous carbon nanosheets with in-plane orderly arranged mesopores and a highly graphitized framework. Angew. Chem.-Int. Edit. 57(11), 2894-2898.

[34] Wang, J.C., Kaskel, S., 2012. Koh activation of carbon-based materials for energy storage. J. Mater. Chem. 22(45), 23710-23725.

[35] Wang, S.R., Dai, G.X., Yang, H.P., Luo, Z.Y., 2017b. Lignocellulosic biomass pyrolysis mechanism: A state-of-the-art review. Progress in Energy and Combustion Science 62, 33-86.

[36] Wu, Y., Cao, J.-P., Zhao, X.-Y., Hao, Z.-Q., Zhuang, Q.-Q., Zhu, J.-S., Wang, X.-Y., Wei, X.-Y., 2017. Preparation of porous carbons by hydrothermal carbonization and koh activation of lignite and their performance for electric double layer capacitor. Electrochim. Acta 252(Supplement C), 397-407.

[37] Xia, S., Xiao, H., Liu, M., Chen, Y., Yang, H., Chen, H., 2018. Pyrolysis behavior and economics analysis of the biomass pyrolytic polygeneration of forest farming waste. Bioresour. Technol.

[38] Xin, S.Z., Yang, H.P., Chen, Y.Q., Wang, X.H., Chen, H.P., 2013. Assessment of pyrolysis polygeneration of biomass based on major components: Product characterization and elucidation of degradation pathways. Fuel 113, 266-273.

[39] Yang, H.P., Coolman, R., Karanjkar, P., Wang, H.Y., Dornath, P., Chen, H.P., Fan, W., Conner, W.C., Mountziaris, T.J., Huber, G., 2017. The effects of contact time and coking on the catalytic fast pyrolysis of cellulose. Green Chemistry 19(1), 286-297.

[40] Yao, D., Wu, C., Yang, H., Zhang, Y., Nahil, M.A., Chen, Y., Williams, P.T., Chen, H., 2017. Co-production of hydrogen and carbon nanotubes from catalytic pyrolysis of waste plastics on ni-fe bimetallic catalyst. Energy Conversion and Management 148(Supplement C), 692-700.

[41] Yao, D., Zhang, Y., Williams, P.T., Yang, H., Chen, H., 2018. Co-production of hydrogen and carbon nanotubes from real-world waste plastics: Influence of catalyst composition and operational parameters. Applied Catalysis B-Environmental 221, 584-597.

[42] Zakzeski, J., Bruijnincx, P.C.A., Jongerius, A.L., Weckhuysen, B.M., 2010. The catalytic valorization of lignin for the production of renewable chemicals. Chemical Reviews 110(6), 3552-3599.

[43] Zhu, K.R., Chen, C.L., Xu, M.W.C., Chen, K., Tan, X.L., Wakeel, M., Alharbi, N.S., 2018. In situ carbothermal reduction synthesis of fe nanocrystals embedded into n-doped carbon nanospheres for highly efficient u(vi) adsorption

and reduction. Chem. Eng. J. 331, 395-405.

[44] Zhu, Q.L., Xia, W., Akita, T., Zou, R.Q., Xu, Q., 2016. Metal-organic framework-derived honeycomb-like open porous nanostructures as precious-metal-free catalysts for highly efficient oxygen electroreduction. Adv. Mater. 28(30), 6391-+.
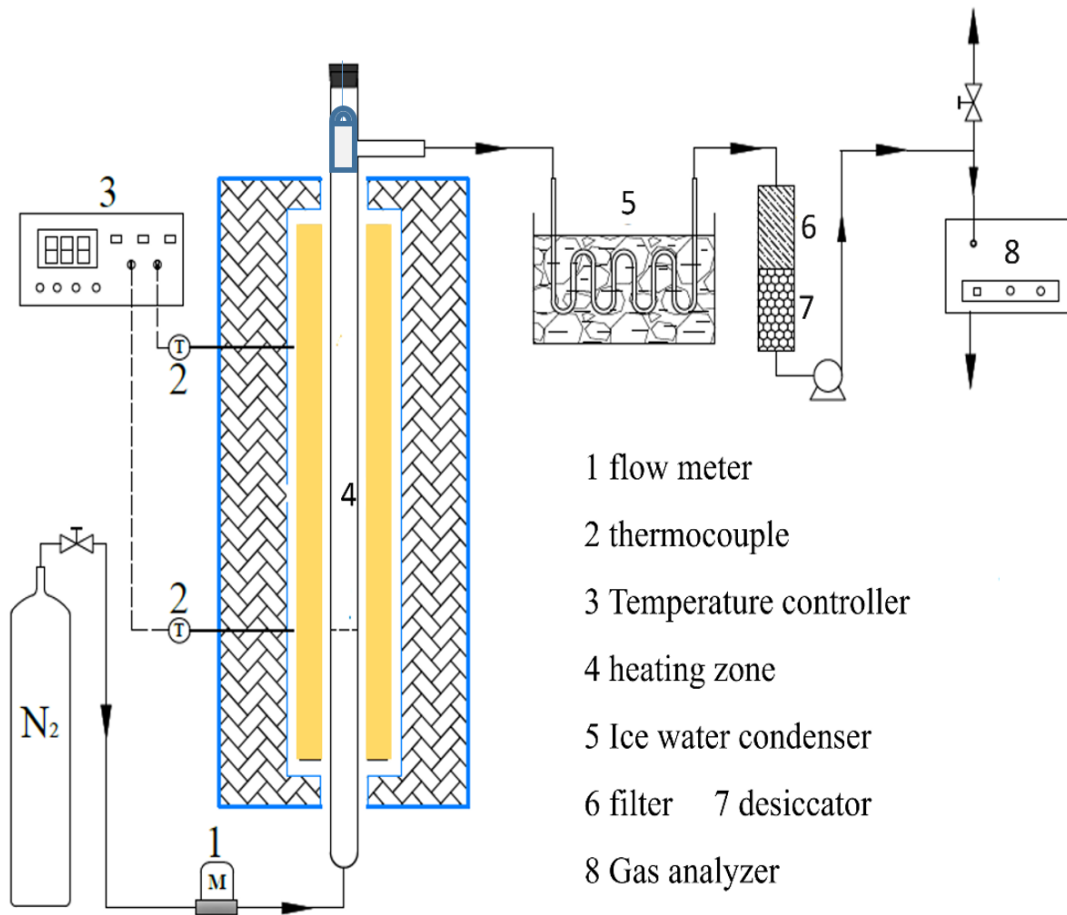
Figure captions

Figure 1. Schematic diagram of biomass pyrolysis system

Figure 2. Temperature-dependent yields of compounds produced by pyrolysis of Chinese chestnut shells.

Figure 3. Effects of temperature and Fe presence/absence on the formation of gaseous products during the pyrolysis of Chinese chestnut shells.

Figure 4. Van Krevelen diagram of solid char produced by pyrolysis of Chinese chestnut shells.

Figure 5. Pore size distributions of solid chars obtained at (a) 400, (b) 500, (c) 600, and (d) 700 and 800 °C in the absence and presence of Fe.

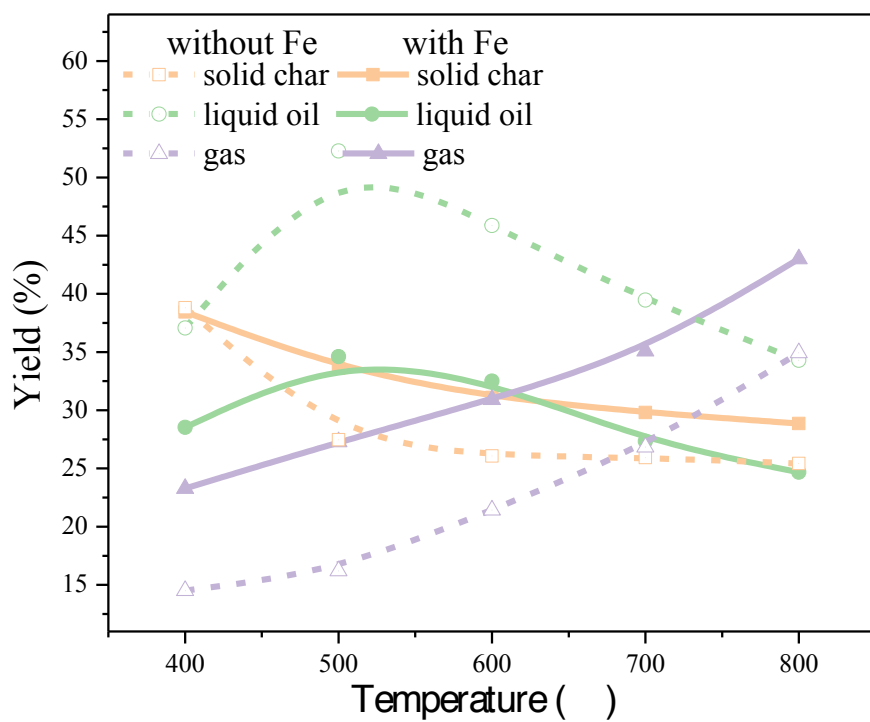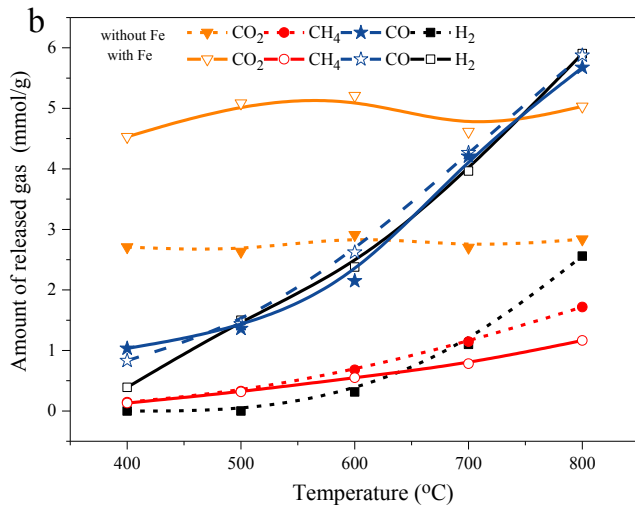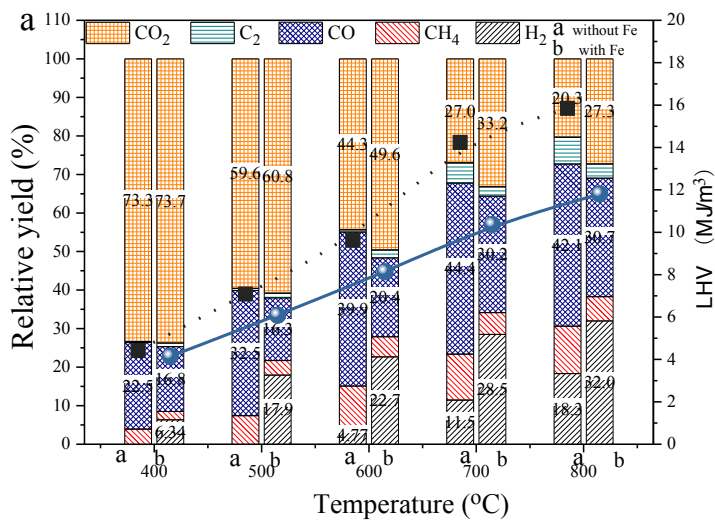Figure 1. Schematic diagram of biomass pyrolysis system

1 flow meter
2 thermocouple
3 Temperature controller
4 heating zone
5 Ice water condenser
6 filter   7 desiccator
8 Gas analyzer

Figure 2. Temperature-dependent yields of compounds produced by pyrolysis of

Chinese chestnut shells

Figure 3. Effects of temperature and Fe presence/absence on the formation of gaseous products during the pyrolysis of Chinese chestnut shells.
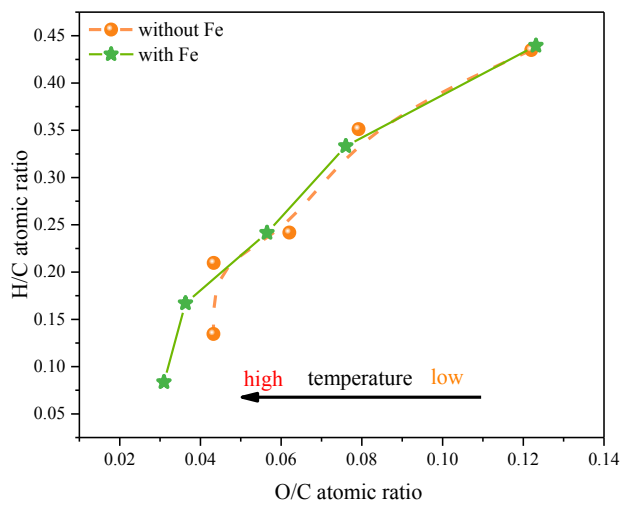
Figure 4. Van Krevelen diagram of solid char produced by pyrolysis of Chinese chestnut shells
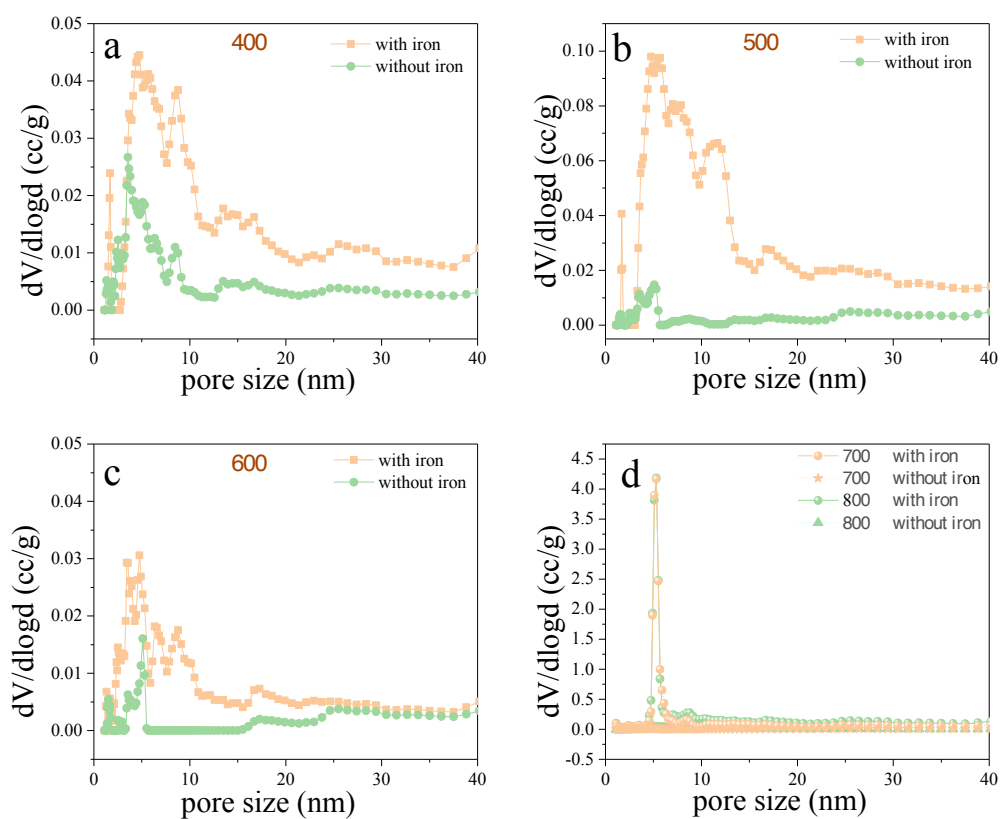
Figure 5. Pore size distributions of solid chars obtained at (a) 400, (b) 500, (c) 600, and (d) 700 and 800 °C in the absence and presence of Fe.

Table 1 the organics in liquid oil.

Compounds	Content (%)									
	Without Fe					With Fe				
Pyrolysis temperature (°C)	400	500	600	700	800	400	500	600	700	800
acids	**23.85**	**24.53**	**27.67**	**34.94**	**57.40**	**38.38**	**31.95**	**34.66**	**42.82**	**67.51**
Acetic acid	20.56	22.29	24.98	31.86	55.31	35.31	31.95	33.15	42.82	67.51
Acetic acid, 2-(5-aminotetrazol-1-yl)-, ethyl ester	3.30	2.24	2.69	3.08	2.09	3.07		1.51		
furans	**13.80**	**10.45**	**9.36**	**8.03**	**12.21**	**16.87**	**12.96**	**12.48**	**11.66**	**4.39**
Furfural	11.78	10.45	9.36	8.03	12.21	12.93	10.08	9.72	8.88	4.39
5-methyl-2-Furancarboxaldehyde	2.01					3.94	2.89	2.76	2.78	
phenols	**9.43**	**7.62**	**4.93**	**5.29**	**9.76**	**3.15**	**3.18**	**2.64**	**4.82**	**4.13**
Phenol				2.23	4.45	1.29	1.44	1.61	3.13	4.13
Phenol, 2-methoxy-	3.94	2.89	3.69		2.15	1.86	1.74	1.03	1.68	
p-Cresol	1.45	1.14	1.24	3.07	3.16					
Phenol, 2,6-dimethoxy-	4.04	3.59								
ketones	**4.68**	**3.79**	**1.08**	**1.72**	**4.18**	**11.27**	**8.86**	**8.11**	**8.61**	**5.13**
2-Propanone, 1-hydroxy-				1.72	2.48	3.25	2.54	2.52	1.14	2.93
2-Pentanone, 4-hydroxy-4-methyl-					1.70	1.51	1.47	1.37	2.07	2.20
1,2-Cyclopentanedione, 3-methyl-						5.08	4.84	4.23	5.40	0.00
4H-Pyran-4-one, 3,5-dihydroxy-2-methyl-	4.68	3.79	1.08			1.44				
sugars	**48.24**	**53.61**	**56.95**	**50.02**	**16.45**	**30.33**	**43.05**	**42.11**	**32.09**	**18.84**
1,4:3,6-Dianhydro-.alpha.-d-glucopyranose	1.71	1.42	1.65	2.14	1.55	1.44	1.49	1.78	3.37	
.beta.-D-Glucopyranose, 1,6-anhydro-	43.15	49.43	52.56	43.72	14.90	28.89	39.85	38.72	28.72	18.84
1,6-Anhydro-.alpha.-d-galactofuranose	3.37	2.76	2.74	4.16	0.00	0.00	1.71	1.61		

Table 2. Texture properties of samples obtained at different temperature

Sample	Temperature (°C)	Surface area (m^2/g)	Total pore volume (cc/g)	Micropore area (m^2/g)	External area (m^2/g)
without Fe	400	31.62	0.019	~	31.62
	500	73.288	0.044	53.219	20.069
	600	92.241	0.0582	65.352	26.889
	700	81.377	0.0558	54.526	26.851
	800	59.08	0.0581	16.230	42.85
With Fe	400	38.035	0.048	~	38.035
	500	62.892	0.061	~	62.892
	600	195.876	0.095	163.928	31.948
	700	299.248	0.382	91.579	207.669
	800	329.106	0.4591	107.352	221.754